WELDING RESEARCH

SUPPLEMENT TO THE *WELDING JOURNAL,* FEBRUARY 2007
Sponsored by the American Welding Society and the Welding Research Council

A Methodology for Prediction of Fusion Zone Shape

This study proposes a methodology for prediction of fusion zone shape that is applicable not only for bead-on-plate welds, but also for T-joint fillet welds

BY N. OKUI, D. KETRON, F. BORDELON, Y. HIRATA, AND G. CLARK

ABSTRACT. This study presents a semiempirical methodology for prediction of fusion depth and width in the gas metal arc welding process. The semiempirical methodology is based on the theoretical heat conduction solution of a moving point heat source with appropriate corrections obtained through experimentation. The corrections reduce the systematic errors observed when theoretical calculations and experimental fusion depth and width measurements are compared. The method uses an applied regression analysis by the least squares method for estimating these errors. The resulting prediction of fusion depth and width by the semiempirical model shows good agreement with experiments for bead-on-plate welds. The methodology is also applicable to T-joint fillet welding with appropriate heat distribution ratio to web and flange. Since this methodology does not require complicated or excessive computation, it is especially useful for actual welding process applications. It will also provide a robust approach to adaptive welding, as well as stabilizing weld quality. A similar welding process model for materials other than steel, such as aluminum alloys and stainless steel, can be developed through the same approach as proposed here with some ancillary experimentation.

Introduction

Prediction of fusion in welding is essential for obtaining adequate joining qualities and increasing productivity. Intelligent automated welding processes require adaptive control technologies that can predict weld fusion in a simple and easy manner. The purpose of this study is to present a practical methodology for the prediction of fusion in welding.

For the prediction of fusion in welding, there are a number of published numerical solutions based on heat conduction models (Refs. 1–5). Although the heat conduction solution provides a fairly accurate prediction of temperature in areas outside the fusion zone, it exhibits errors in fusion zone shape predictions. A major reason is that fluid flow dominates heat transfer in the weld pool, and consequently, determines the fusion zone shape. The various driving forces acting on the fluid flow in the weld pool include electromagnetic force, arc plasma flow, surface tension, and buoyancy. These were investigated in a number of simulation studies of fluid flow caused by interaction of various driving forces, as well as on the effect of individual driving forces (Refs. 6–18, 23).

Currently, simulation software development for welding processes is focused on obtaining supporting tools for production, such as development of a smart welding machine, an intelligent welding robot, and also on education and training for welding engineers and welders (Ref. 13). Generally, the weld heat flow and fluid flow are computed through equations of continuity, energy, and motion. The effects of individual driving forces are then evaluated separately, as well as in combination. More detailed and accurate models are being developed and validated, in parallel with investigation of weld pool convection.

Despite all these efforts, there still remains some difficulties in the practical application of numerical models. The numerical model simulations require many calculations for simultaneously solving the coupled fluid and energy equations taking into account all the phenomena occurring in the weld pool. Furthermore, essential data for high-temperature-dependent properties of material, such as the weld surface tension gradient and viscosity gradient, are inadequately defined at present (Ref. 18). The inclusion of many complex parameters has limited the utilization of simulation software in current production applications, especially for fluid flow in T-joint fillet welding. Our knowledge with regard to the T-joint is still limited.

In view of realizing a production-friendly predictive model, the present study adopts a method that obtains an approximation of the weld interface with the heat conduction solution by adopting semiempirical corrections obtained from systematic experiments. A reasonable estimate of the temperature distribution can be obtained via the heat conduction solutions when boundary conditions are given. For example, the following are important factors:

- welding parameters such as heat intensity and traveling speed,
- kinds of materials,

KEYWORDS

Gas Metal Arc Welding
Bead-on-Plate Welds
T-Joint Fillet Welds
Fusion Depth
Fusion Width

*N. OKUI and F. BORDELON (f*rank.bordelon@uno.edu*) are with the University of New Orleans Gulf Coast Region Maritime Technology Center, Avondale, La. D. KETRON is with the Edison Welding Institute, Columbus, Ohio. Y. HIRATA is with The Osaka University, Osaka, Japan. G. CLARK is with The Ohio State University, Columbus, Ohio.*

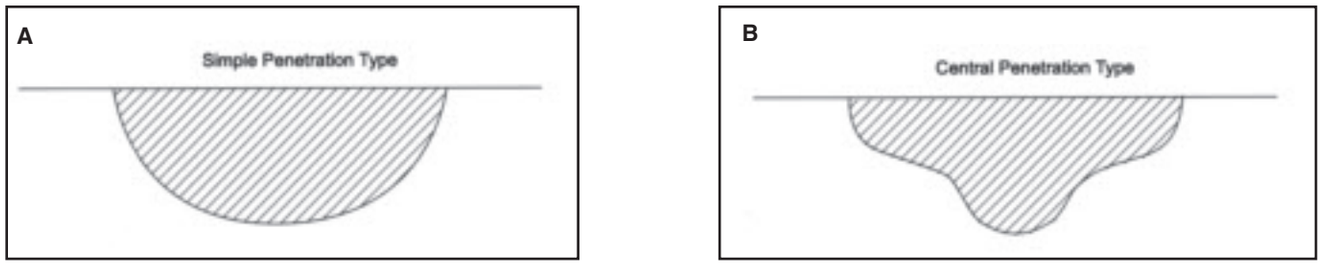

Fig. 1 — Three typical cross-sectional penetration types in arc welding

• size of material, finite/infinite of base metal, plate thickness, joint edge shapes.

The fusion zone shape calculated by the heat conduction solution, however, will have some errors from actual welding. In the present study, the fusion depth and width are first estimated using the moving point heat source solution and then corrected using regression equation obtained from bead-on-plate welding experiments. Since the errors between the theoretical calculations and experiments are systematic, the regression equations corrections provide accurate estimates for the prediction of fusion shape. This study also investigates the fusion in T-joint fillet welds by applying the same methodology with appropriate distribution ratio of heat intensity on web and flange. The predictions are in good agreement with the experiments providing a simple and practical method for predicting fusion depth and width in bead-on-plate and T-joint fillet welds.

Mechanism of Fusion in Gas Metal Arc Welding

Fluid flow in the weld pool is the major factor to determine the fusion zone shape (Refs. 6, 17). The driving forces acting on the fluid flow vary with welding current, arc length, welding speed, and shield gas, resulting in large variations in the fusion zone shape. Nevertheless, three fusion zone cross-section shapes in Fig. 1 are frequently adopted (Refs. 16, 19, 20). They consist of 1) simple penetration type, 2) central penetration type, and 3) peripheral penetration type. In the simple penetration type, the cross-sectional weld interface has a semicircular or elliptical shape. It tends to appear in welding with a lower current and a shorter arc. The temperature distribution in this simple penetration type closely resembles the temperature distribution calculated through the moving point heat source assumption (Ref. 20).

The central penetration type frequently appears under heavy current. A strong plasma stream deeply depresses the molten pool at its center, resulting in deeper fusion at the center (Ref. 20). Surface-active elements such as sulfur and oxygen can also make the fusion deeper by altering surface tension gradients on the weld pool surface and thereby, changing the magnitude and/or direction of fluid flow in the weld pool (Refs. 11, 12).

The peripheral penetration type is observed when a long arc length is held for a long time. The formation of this type may be explained by internal convection in the molten pool. As the surface temperature at the center of the molten pool becomes higher than the peripheral zone, a surface flow from the center to the peripheral zone is enhanced by the surface tension gradient (Ref. 20).

Heat transfer along the welding direction also affects the determination of the horizontal fusion zone shape. Arc forces tend to push liquid metal toward the rear boundary of the weld pool. In addition, the surface tension gradient also enhances fluid flow in the same direction. This trend becomes significant at both a higher current and a higher speed of welding providing increase of fusion depth and decrease of width (Refs. 1, 21, 22).

A Moving Point Heat Source Solution

This study begins with the heat conduction solution. It provides an approximation of fusion zone shape through a simple calculation assuming a moving point heat source. It can be used to calculate fusion volume, fusion width and depth, weld ripple lag, and average temperature of the weld pool (Ref. 1). It has also been utilized to calculate the heat capacity and average temperature of the leading part and trailing part of the weld pool separately (Ref. 2). The general assumptions below are used in a moving point heat source solution (Ref. 2).

Only heat conduction by a moving point heat source is considered in heat transfer. The surface of the weld pool is assumed to be flat. Material properties such as heat conductivity, specific heat, and specific gravity are assumed to be constant. Latent heat is neglected. A semi-infinite plate geometry is assumed.

In addition, the present study includes heat dissipation by means of radiation and atmospheric convection from the plate surface in defining the arc efficiency.

Taking the position of a point heat source as the origin O, and the welding direction as x axis, and the distance of any point from the x axis as r, Z is defined as Z (x, r), the temperature at the point Z (x, r) in an infinite body is expressed as Equation 1 (Refs. 1, 2), where an arc is assumed as a moving point heat source.

$$T = \frac{q}{2\pi\lambda} \cdot \frac{e^{-\frac{v}{2k}\left(x+\sqrt{x^2+r^2}\right)}}{\sqrt{x^2+r^2}} \qquad (1)$$

where T = temperature rise at the point Z [K]; q = heat intensity [J/ s]; v = welding speed [m/ s]; λ = heat conductivity [W/ (m · K)]; κ = thermal diffusivity [m^2/ s] {$\kappa=\lambda /(c \cdot p)$}; c = specific heat [J/ (kg · K)]; ρ = density [kg/ m^3].

Let the welding conditions be defined by an operating parameter n[1] — a quantity related to the product of heat intensity q and welding speed v

$$n = \frac{q}{2\pi\lambda} \cdot \frac{v}{2\kappa} \cdot \frac{1}{T_f} \qquad (2)$$

1. *The operating parameter* n *will prepare more accurate parameter for evaluating fusion of base material in welding. Many works use the parameter of the Heat Input [J/(m/s)]; however, the relation of fusion and heat intensity may express some more errors, because more heat will be dissipated to the adjacent base metal without fusing in a welding with slower speed.*

Table 1 — Welding Parameters

	(1) Bead-on-plate welding						(2) T-joint fillet welding						
Welding Position	Welding Current A	Voltage V	Speed m/s	Plate Thick mm	Weaving Width mm	Operating Parameter	Welding Current A	Voltage V	Speed m/s	Plate Thick mm	Weaving Width mm	Operating Parameter	Root Opening mm
Horizontal	231.9	25.1	0.0118	12	-	17.4	272.9	26.4	0.0118	12	-	21.5	0.0
	225.6	25.0	0.0071	5	-	10.2	266.4	23.5	0.0063	12	-	9.9	0.4
	201.5	28.4	0.0118	12	-	17.0	320.8	26.4	0.0063	12	-	13.4	0.5
	193.8	25.2	0.0118	5	-	14.6	262.6	23.9	0.0063	12	0.7	9.9	0.3
	232.6	24.9	0.0118	5	-	17.3	253.7	23.9	0.0063	12	2.0	9.6	0.1
	195.3	28.4	0.0063	5	-	8.8							
	196.1	25.3	0.0063	12	-	7.9							
	229.8	28.2	0.0063	12	-	10.3							
	241.8	23.8	0.0063	12	0.7	9.1							
	231.7	23.9	0.0063	12	2.0	8.8							
Vertical	138.3	22.3	0.0050	12	-	3.7	147.4	21.9	0.0050	12	-	3.8	0.1
	138.7	22.1	0.0033	5	-	2.4	143.1	21.2	0.0033	12	-	2.4	0.1
	119.8	23.0	0.0050	12	-	3.3	167.7	22.0	0.0033	12	-	2.9	0.0
	121.2	22.2	0.0050	5	-	3.2	138.8	20.7	0.0033	12	0.7	2.3	0.4
	144.3	23.0	0.0050	5	-	4.0	137.0	20.7	0.0033	12	2.0	2.2	0.4
	119.4	23.0	0.0033	5	-	2.2							
	118.9	22.2	0.0033	12	-	2.1							
	144.2	23.0	0.0033	12	-	2.6							
	134.0	21.2	0.0033	12	0.7	2.2							
	136.0	20.9	0.0033	12	2.0	2.3							
Overhead	197.9	23.0	0.0077	12	-	7.8	203.8	23.9	0.0077	12	-	8.3	0.0
	197.7	22.9	0.0050	5	-	5.0	189.3	21.7	0.0050	12	-	4.6	0.2
	171.5	25.3	0.0077	12	-	7.4	220.3	24.0	0.0050	12	-	5.9	0.2
	169.0	23.2	0.0077	5	-	6.7	199.6	21.9	0.0050	12	0.7	4.9	0.1
	198.4	25.1	0.0077	5	-	8.5	198.5	22.0	0.0050	12	2.0	4.9	0.2
	169.3	25.3	0.0050	5	-	4.8							
	171.8	23.2	0.0050	12	-	4.4							
	195.4	25.2	0.0050	12	-	5.5							
	165.2	22.3	0.0050	12	0.7	4.1							
	171.5	22.0	0.0050	12	2.0	4.2							

where T_f = temperature rise to melting point; $T_f = T_m - T_0$, T_m : melting point (T_m = 1808 K, in the case of steel); T_0 = room temperature.

Let the parameters *x, r,* and *z* be represented by dimensionless parameters multiplying by *v*/2k

$$X = x \cdot \frac{v}{2\kappa},\ R = r \cdot \frac{v}{2\kappa},\ Z = z \cdot \frac{v}{2\kappa}$$

Substituting Equation 2 in Equation 1, one obtains

$$\frac{T}{T_f} \cdot \frac{1}{n} = \frac{1}{\sqrt{X^2 + R^2}} \cdot e^{-\left(X + \sqrt{X^2 + R^2}\right)} = \frac{1}{Z} \cdot e^{-(X+Z)} \qquad (3)$$

Equation 3 gives the fusion temperature contour in welding when $T = T_f$ is substituted. Figure 2 shows a theoretical outer elliptical line of molten pool, where points S, M, P, and M' are calculated by Equations 4, 5, 6, and 7 with $n = 7.86$.

In Fig. 2, M-M' is the maximum fusion width. One will obtain by the condition of $dR/dX = 0$ on the isothermal contour expressed by Equation 3, where $T = T_f$

$$X_m = -\frac{Z^2 m}{1 + Z_m} \qquad (4)$$

$$Z_m = \sqrt{X^2 m + R^2 m} \qquad (5)$$

$$Z_m \cdot e^{\frac{Z_m}{1+Z_m}} = n \qquad (6)$$

In addition, for R = 0, one obtains point S (X_1) and P ($-X_2$) in Equation 3.

$$\left.\begin{aligned} X_1 \cdot e^{2X} 1 &= n \\ X_2 &= n \end{aligned}\right\} \qquad (7)$$

This results in a semicircle with radius R for the cross-sectional isothermal contour for the weld pool.

Christensen et al. (Ref. 1) showed the experimental fusion width is greater than the calculated width, and the trend is reversed in fusion depth. The errors in the fusion depth and width calculations are attributed to the effects of heat source properties and weld pool convection. The increased arc forces at the high value of *n* also introduce preferential currents flowing from the crater in directions downward and toward the rear boundary of the pool (Ref. 1).

In addition, the following are constants adopted in the theoretical calculations in this study:

λ: Heat conductivity 33.47 [W/(m· K)]
c: Specific heat 878.6 [J/(kg· K)]
ρ: Density 7600 [kg/m^3]
κ: Thermal diffusivity 5×10^{-6} [m^2/s], $\kappa = \lambda/(c \cdot \rho)$
T_f: Temperature rise to melting point 1500 [K]

Experimental Procedures

The experimental welding process employed in this study is bead-on-plate and T-joint fillet with gas metal arc welding (GMAW), with the following conditions: welding current for horizontal position, 193–242 A, welding speed, 0.0063–0.0118 m/s; for vertical position, 120–145 A, welding speed, 0.0033–0.005 m/s; for overhead position, 169–198 A, welding speed 0.0077–0.0050 m/s; consumable welding wire, SF-1 seamless flux cored

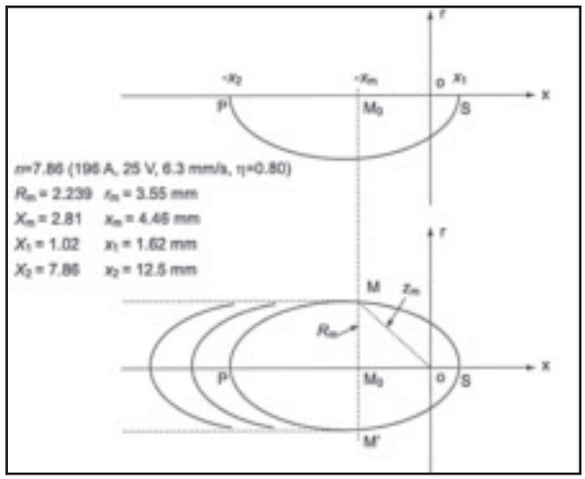

Fig. 2 — Theoretical weld pool outer line by a moving point heat source solution.

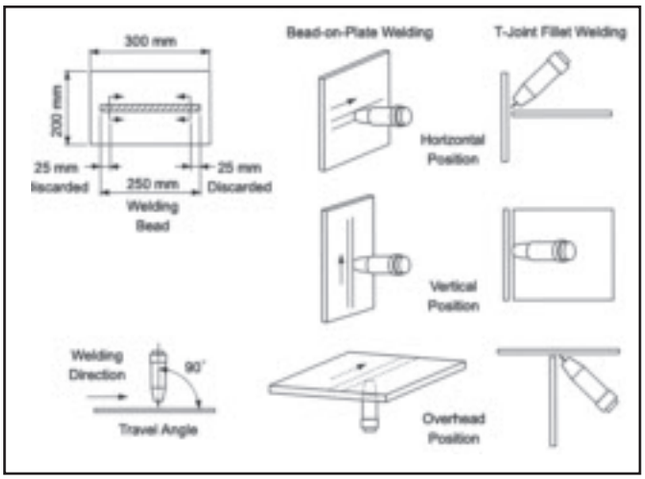

Fig. 3 — Test specimen assembly and welding orientation.

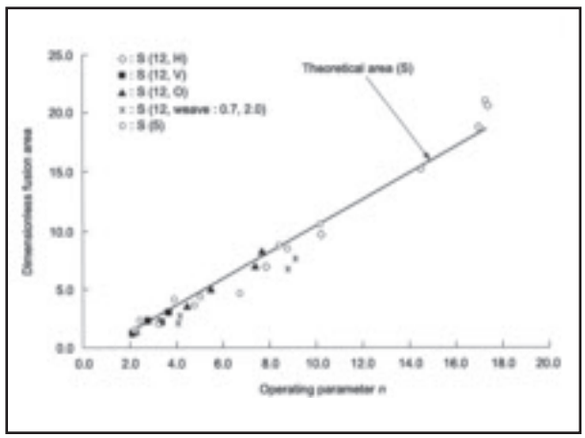

Fig. 4 — Fusion area (bead-on-plate welding, 5- and 12- mm plate thicknesses; welding positions (H) horizontal, (V) vertical, (O) overhead; 0.7- and 2.0-mm weaving width). The arc efficiency was estimated as 80%, 75%, and 70% for H, V, and O, respectively, from comparing the theoretical cross-section area with experiments.

wire, 1.2 mm diameter; shielding gas 100% CO_2, flow rate 0.33 L/s. Table 1 lists welding parameters applied in this study. They were selected so that the combination represents the statistic sampling. The values of operating parameter n are in the range of 2.1 ~ 21.5. The base metal is carbon steel the size of 200 × 300 mm; plate thicknesses 12 mm and 5 mm, thermally insulated with ceramic block from the experimental slab. Figure 3 shows the assembly of the test specimen and welding orientation. About 25 mm of both ends of the welding bead are discarded, and two sections taken from the center section are used for the fusion area, depth, and width measurements.

Estimation of Arc Efficiency

Christensen et al. (Ref. 1) found the weld pool volumes derived from the moving point heat source solution are in good agreement with experiments. In the present study, the arc efficiency was estimated from comparing the theoretical fusion cross-section area 1⁄2pRm2 with experiments. The experimental fusion area s was converted to a dimensionless basis

$$S = \left(\frac{v}{2k}\right)^2 \cdot s$$

The sampled fusion area for the estimation of arc efficiency was obtained from bead-on-plate welds with a plate thickness of 12 mm.

In the gas metal arc welding processes, heat dissipates into the atmosphere by means of heated shield gas dissipation, spatter, radiation, and atmospheric convection from the surface of weld pool and base material. Since welding current and speed, shape of weld pool, and volume of deposited metal have an effect on the heat dissipation, the welding orientation is one of the major factors that affect arc efficiency. The arc efficiency was estimated as 80% for horizontal position, 75% for vertical position, and 70% for overhead position. The theoretical fusion area calculated with these values agreed well with the experimental measurement in Fig. 4. The estimated arc efficiency values are consistent with those obtained by Christensen (Ref. 1) and are applicable to subsequent calculations of fusion depth and width.

Predicting the Fusion Depth and Width in Bead-on-Plate Welds

Figure 5 shows a typical cross-sectional macrostructure. It has a fusion zone shape representative of the other specimens of the simple penetration type (a).

The experimental measured fusion depth d and width w are converted to dimensionless basis

$$D = \frac{v}{2k} \cdot d,\ W = \frac{v}{2k} \cdot w$$

Figure 6 shows a comparison of the theoretical and experimental fusion depth and width in bead-on-plate welds. As postulated earlier, the theoretical fusion depth appears to be larger than the experiments; conversely, the width appears smaller. The errors between them seem systematic for both fusion depth and width for the wide range of operating parameter n; however, the fusion depth in plate thickness 5 mm appears wider than range scattering.

This study applies the least squares regression to welding a 12-mm plate without weaving to avoid any influences from weaving or a thinner plate using elasticity model. The data were felled to a regression equation $y = a \cdot x^b$. Taking the logarithm on both sides, one obtains:

$$\ln y = \ln a + b \cdot \ln x \qquad (8)$$

Here, y is the dependent variable representing fusion depth or width and x is the independent variable representing operating parameter n. The experimental

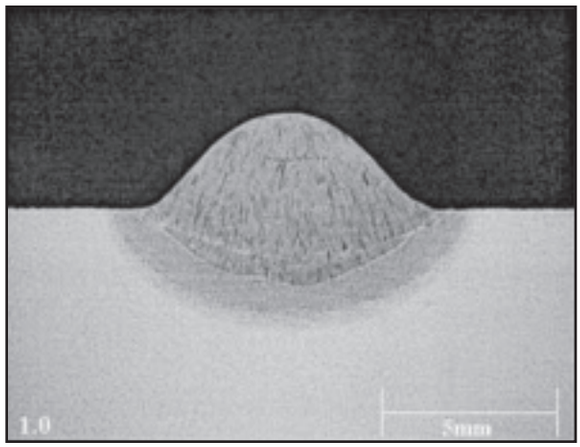

Fig. 5 — Example of cross-sectional macrostructure in bead-on-plate welding (12-mm-thick plate, no weaving, overhead position, n = 7.78, 198 A, 23 V, 7.7 mm/s, h = 70%). The macrostructure has a fusion zone shape representative of the other specimens of the simple penetration type.

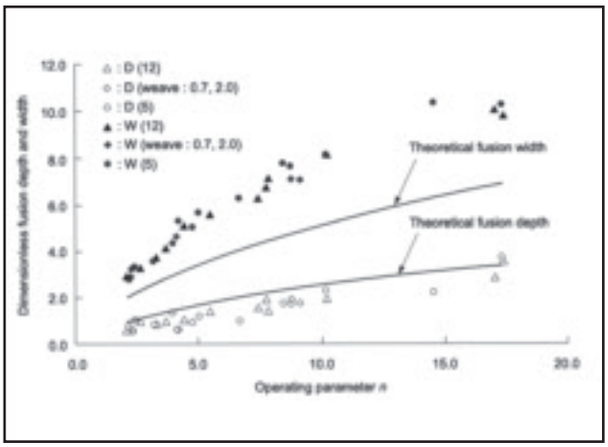

Fig. 6 — Fusion depth and width in bead-on-plate welding (fusion depth D, fusion width W, 12- and 5-mm-thick plates, 0.7- and 2.0-mm weaving widths). Welding positions include H, V, and O.

measured data were analyzed through a linear regression with Equation 8. The regression equations for fusion depth and width are expressed as follows:

$$D^* = 0.4175 \cdot n^{0.6996} \quad (D^*\text{Estimator}^2 \text{ for fusion depth}) \qquad (9)$$

$$W^* = 1.9737 \cdot n^{0.5889} \quad (W^*\text{Estimator}^2 \text{ for fusion width}) \qquad (10)$$

The correlations of determination R^2 are 0.945 and 0.984 for fusion depth and width, respectively. The other test statistics for the regression analysis are listed in Table 2.

Figure 7 shows the estimated fusion depth and width calculated by Equations 9 and 10 along with the experimental data. The regression equations show good agreement with the experiments. An experimental fusion depth in higher *n* value appears slightly larger than required by regression equation, and conversely, width is smaller. This tendency is consistent with the Christensen et al. results (Ref. 1). The estimation by the regression equations can predict well both fusion depth and width for the operating parameter less than 15.

It is well known that the temperature rise in the base material when welding a thinner plate is greater than in a thicker plate. This study also examined fusion area, depth, and width for a 5-mm plate thickness. As observed in Fig. 4, the experimental fusion area in the 5-mm plate also agrees with the theory, as well as in the 12-mm thickness. Figure 6 shows fusion depth and width in the 5-mm thickness. The fusion depth, however, seems to have larger fluctuations than in the 12-mm thickness. The reason for this fluctuation is discussed later. Figure 4 also shows the fusion area when welding with a 0.7 and 2 mm weave on a 12-mm plate. The fusion area by welding with weaving is slightly smaller than predicted by the calculation. In Fig. 6, experiments with weaving show good agreement with the regression equations. As known, weaving increases fusion width, and conversely, decreases fusion depth; however, the difference between with/without weaving is not significant when the weaving is less than 2 mm.

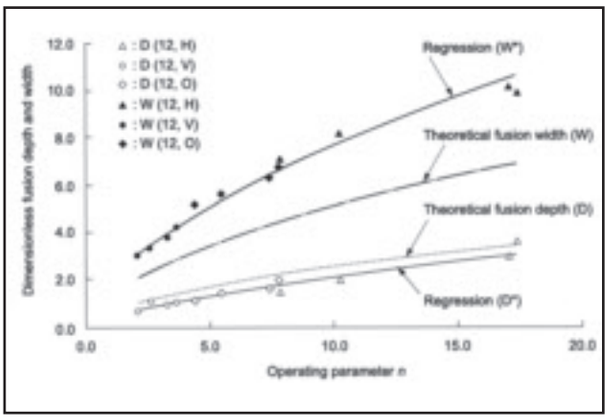

Fig. 7 — Regression of fusion depth and width (bead-on-plate welding, 12-mm-thick plate, no weaving). The correlations of determination are 0.945 and 0.984 for fusion depth and width, respectively.

2. The regression equations can estimate fusion depth and width obtained from statistics analysis.

Predicting the Fusion Depth and Width for T-Joint Fillet Welds

A T-joint consists of two perpendicular plates, which can include different plate positions such as horizontal-vertical or vertical-overhead. The heat flow and fluid flow in T-joint fillet welding is significantly different from bead-on-plate welding. The volume and the shape of weld pool, the direction of plasma stream, and the discontinuity of heat conduction at the abutting surface on the other plate have an effect on the heat transfer and the fusion of each plate. Our knowledge of the T-joint fillet welding process with regard to the heat distribution, fluid flow, and mechanism of fusion is limited at present. Furthermore, there are many error factors in the welding process such as deviations of welding gun position and angle, and root opening. This study investigates fusion area, depth, and width in T-joint fillet welds applying the same regression equations obtained from the bead-on-plate welds.

Figure 8 presents a conceptual diagram of heat flow and fusion zone depth and width in T-joint fillet welding. The purpose of this figure is to illustrate the complexity of the T-joint geometry compared to the bead-on-plate geometry considered previously. For example, the fusion zone may not be symmetric about the point of maximum depth (D) because of asymmetric conditions. The present

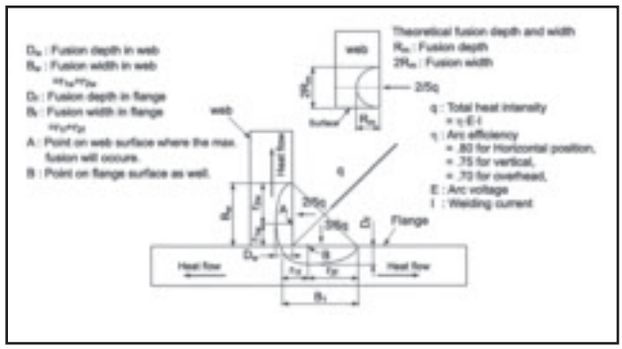

Fig. 8 — Conceptual model of heat flow and fusion in T-joint fillet weld.

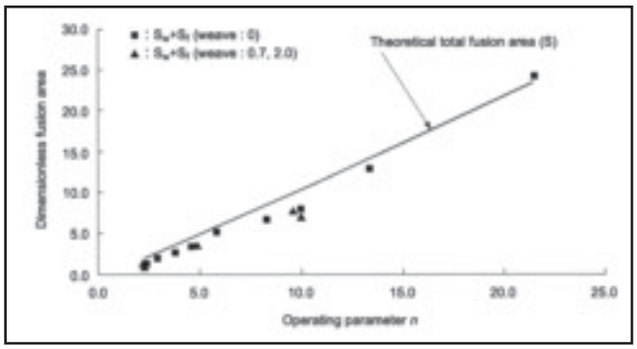

Fig. 9 — Total fusion area in web and flange. Experimental fusion area is a sum of cross-sectional area in web (S_w) and flange (S_f).

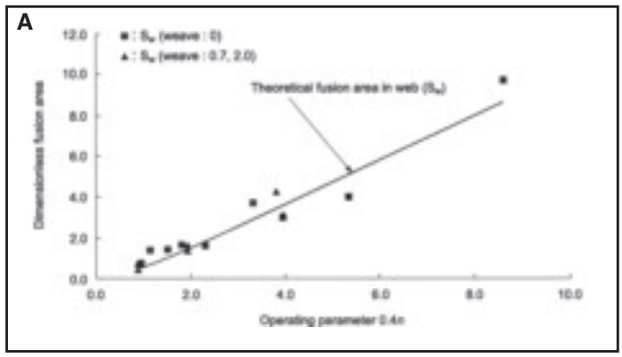

Fig. 10 — Fusion area in web and flange. The heat distribution ratio for theoretical calculation is estimated from the experimental fusion area in web and flange as 2/5: 3/5. A — Fusion area in web; B — fusion area in flange.

Table 2 — Test Statistics of Null Hypothesis Testing

Null Hypothesis Testing (two-tailed test), Population Regression: $y=\beta_1+\beta_2.x$

Testing 1: Fusion depth (D*)		Testing 2: Fusion width (W*)	
Hypothesis	$\beta_2 = 0$	Hypothesis	$\beta_2 = 0$
Alternative hypothesis	$\beta_2 \neq 0$	Alternative hypothesis	$\beta_2 \neq 0$
Significant level	0.01	Significant level	0.01
Test static t	13.14	Test static t	24.96
Percent point	3.11	Percent point	3.11
t > percent point		t > percent point	
Reject		Reject	
Reference	P :6.3 $\times 10^{-6}$ R^2:0.945 F :172.60	Reference	P :3.3 $\times 10^{-8}$ R^2:0.984 F :623.00

work estimates the total area of the fusion zone, not the detailed geometry. The following conditions are assumed:

1) Heat intensity is applied separately to web and flange with appropriate distribution ratio and the fusion is processed separately on each plate by the distributed heat.

2) The fusion area, depth, and width are calculated irrespective of the location of point heat source.

3) Fusion width on the web is designated as the distance from flange surface to outer weld interface on the plate surface.

Although two perpendicular plates have different welding positions, for simplicity, this study applies the same arc efficiency for bead-on-plate welding, i.e., 80% for horizontal, 75% for vertical, and 70% for overhead position.

Figure 9 shows theoretical total fusion area and experimental fusion area, i.e., the sum of the fusion area in web and flange. This figure shows the calculation results are slightly larger than experiments. Since the error is negligibly small, this figure shows the estimated arc efficiency is also applicable to the T-joint fillet welding.

The heat distribution into web/flange is complicated because the mass and shape of molten metal also affects heat transfer in three dimensions along the interface of the two perpendicular plates. In the present experiments, the web and flange are of equal thickness and the welding gun is maintained at a 45-deg angle. Further studies are appropriate to determine the sensitivity to web and flange thicknesses, gun angle, and material. The flange extends in two directions while the web extends in one direction. The temperature difference at the web-flange contact surface is small and more energy flows into the flange. This study found a distribution of 60% into the flange and 40% into the web yielded reasonable results.

Figure 10A and B show the fusion area in web and flange, along with a comparison of the theoretical and experiments. In lower n value, the fusion area of the web appears larger than the calculation, and conversely smaller in the flange. For these welds, the cross-sectional macrostructure shows inclined deposited metal on the web, which implies an offset of welding wire. This offset effects also fusion depth

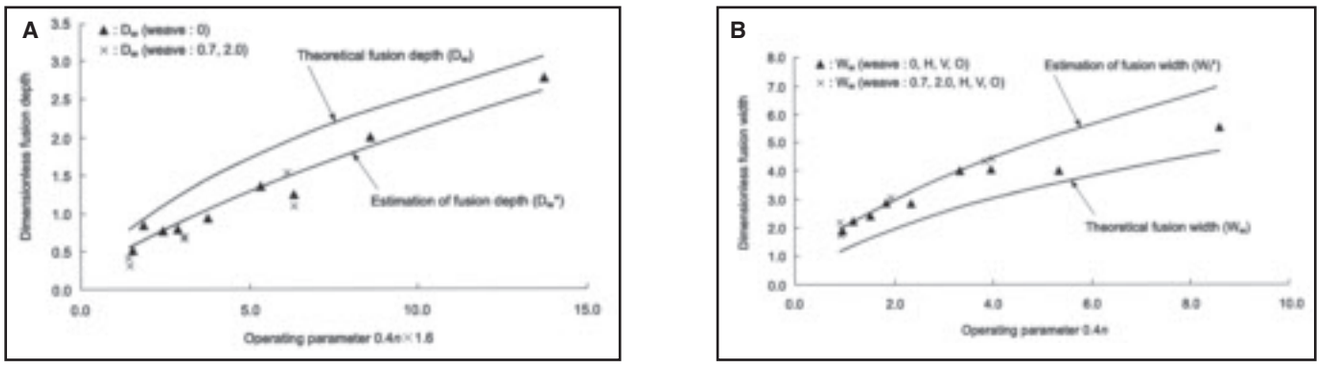

Fig. 11 — Fusion depth and width in web. A — Fusion depth in web. The heat intensity is assumed as 40% of total heat intensity by distribution ration and then multiplied by 1.6 taking the heat reflection into account; B — fusion width in web. The heat intensity is assumed as 40% of total heat intensity by distribution ratio, and the effect of heat reflection is neglected for fusion width.

and width as well as fusion area. By taking this error into account, the calculated fusion area with the distribution ratio agrees well with experiments. The approximate distribution ratio is adopted in the subsequent calculations of fusion depth and width in T-joint fillet welding.

The web in the T-joint also has a finite material surface. In a finite body, the heat does not conduct beyond the surface; it raises the temperature higher than in an infinite body with some heat dissipating outside of the body from the surface. This end condition on temperature rise acts as if the heat reflects at the surface without further conduction. The temperature rise also enhances fusion at the near boundary of the web end surface. As this study adopts the heat conduction solution for an infinite body, the end effect of the surface on the temperature rise is not negligible. This study also includes the effect of heat reflection, so that the calculation meets well with experimental fusion depth. This results in making an assumption that there is an additional 60% of heat intensity. Figure 11A shows estimated fusion depth using the heat intensity $0.4n \times 1.6$ and compares with experimental fusion depth. This assumption of heat intensity results in good agreement with the experiments over the entire range of n values used in this study.

The effect of reflected heat is neglected in the calculation of fusion width. This is due to the outer weld interface on the web having a significant distance from the web end surface. Figure 11B shows that the fusion width calculated with heat intensity $0.4\,n$ is in good agreement with the experiment for lower n values. For higher n values, the deviation between the calculations and experimental fusion width is considerably larger. In horizontal T-joint fillet welding, gravity force deforms the molten metal and it drops on the horizontal plate. This larger quantity of molten metal reduces the fusion width (Refs. 24, 25). Consequently, restrained fusion width in the horizontal plate is attributed to the inclined deposited metal on the horizontal plate. Further studies on the fluid flow in fillet welding are needed to clarify this process.

Figure 12 shows fusion depth and width in the flange. Although the experimental data scattering appears larger than that in the bead-on-plate weld data, the calculation shows fairly good agreement with the experiments.

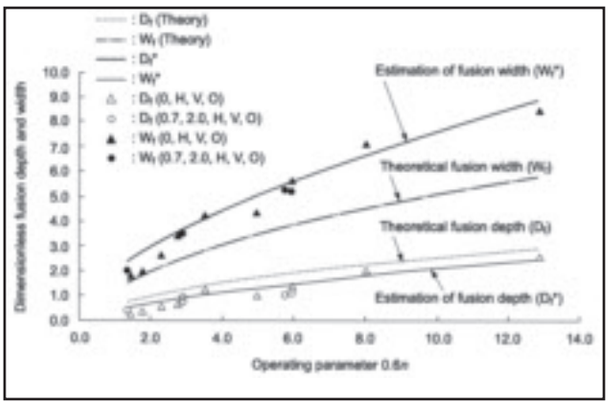

Fig. 12 — Fusion depth and width in flange. D_f (0.7, 2.0 H, V, and O) indicates weaving widths of 0.7 and 2.0 mm, including weaving positions of H, V, and O.

Figure 11A and B, and Fig. 12 also show fusion depth and width with weaving. Generally, weaving will decrease the fusion depth in the web, and conversely, will increase the width; however, the effect of weave with widths of 0.7 and 2.0 mm is not significant for either the web or the flange. (Note: In Fig. 11 Wf* should be Ww*.)

Discussion

Effect of Plate Thickness

Figure 13A and B compares the cross-sectional macrostructure of welding 12- and 5-mm-thick plates, with the same welding parameters. In the 12-mm plate, the boundary of the heat-affected zone (HAZ) appears along the weld interface without the influence of reflected heat. In the 5-mm plate thickness, Fig. 13A shows the HAZ extends to the plate's back surface. In addition, slight deformation is also observed on the plate's back surface, implying the temperature exceeds A_1 transition temperature (about 1023 K or 750°C in steel) at the plate's back surface.

Figure 14 shows isothermal contours of 1023 K (750°C) and 648 K (375°C) calculated using Equation 3, including a comparison with the actual HAZ. As observed in Fig. 14, the HAZ line of actual welding (Fig. 13B) meets well with the theoretical isothermal contour 648 K (375°C) on the plate's back surface. This figure indicates that the temperature on the plate's back surface rises approximately twice as much as theoretical temperature calculated for an infinite body. Namely, the theoretical temperature 1023 K (750°C) on the plate's back surface approximates the weld interface 1773 K (1500°C) in welding thinner plate. It is postulated that the fusion depth increases abruptly when the theoretical temperature contour of 1023 K (750°C) extends close to the reverse surface. The wider scattering observed in Fig. 6 is consequently attributed to the heat reflection from the plate's back surface.

This heat reflection also affects the fusion depth in the web of T-joint fillet welding. While the assumption of an additional 60% heat intensity provides

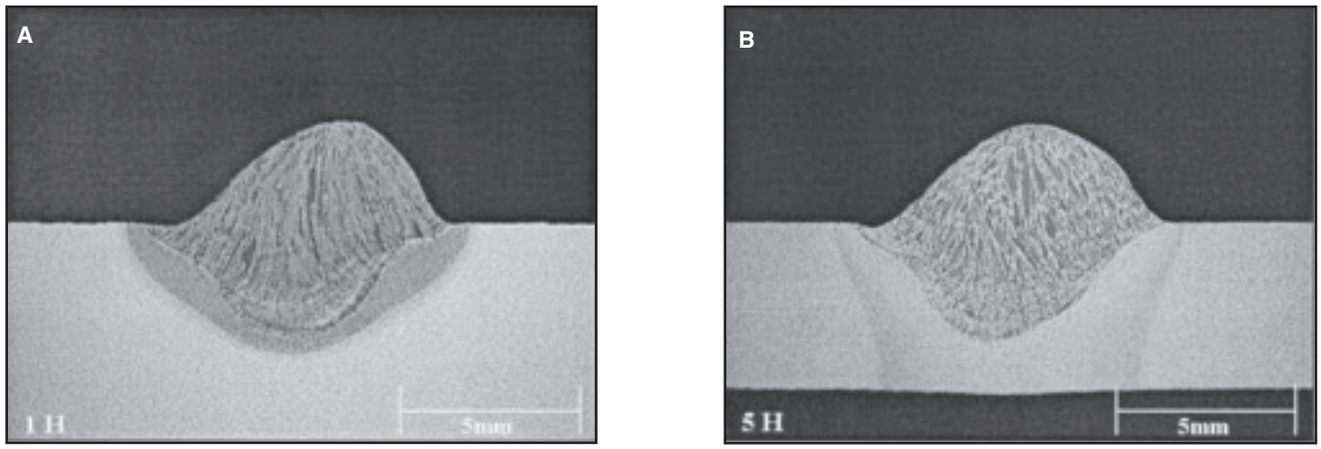

Fig. 13 — Comparison of cross-sectional macrostructure of 12- and 5-mm- thick plates in a bead-on-plate weld. Extended HAZ in the 5-mm plate implies the excessive temperature rise caused by the effect of the plate's back surface. A — Horizontal position, n = 17.4, 12-mm-thick plate, 232 A, 25.1 V, 11.8 mm/s; B — horizontal position, n = 17.4, 5-mm-thick plate, 233 A, 24.9 V, 11.8 mm/s.

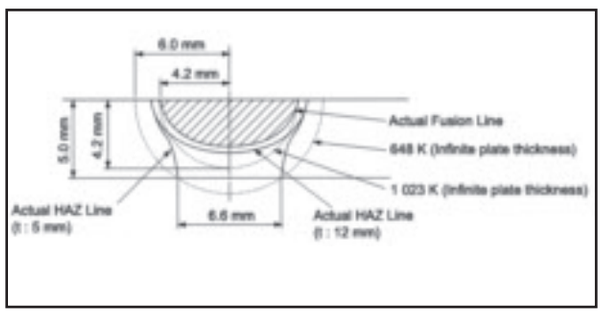

Fig. 14 — Comparison of isothermal contour using a moving point heat source and HAZ line while actually welding (n = 17.3, 233 A, 24.9 V, 11.8 mm/s). The isothermal contour of 648 K (375°C) intersect the actual HAZ line (750°C), implying that the temperature at the plate's back surface is raised as high as twice of theoretical temperature calculated for an infinite body.

good agreement with the whole range of this experiment, for large values of n (n = 21), adopting a value of 80% gives better agreement. This is understandable since the point of maximum fusion depth is located closer to the boundary of the material end surface with a higher value of operating parameter n.

Weaving

Generally, weaving will have an effect on fluid motion in the weld pool, thereby decreasing fusion depth and increasing fusion width. The regression analysis indicate results there is little effect of the weaving for width under 2 mm. The effect of weaving seems to be concealed with the other driving forces in the weld pool when the weaving width is smaller than 2 mm. While a wider weaving width may increase the fusion width and decrease the fusion depth by changing the heat source properties, and the fluid flow in the weld pool, this requires further investigation.

Applicable Range of the Semiempirical Methodology

This study has presented the methodology and results for correcting the moving point heat source solution using bead-on-plate weld data. Because the errors are caused by the fluid flow in the weld pool that varies with different welding conditions, the estimates from the model will give an error because the fusion zone shape differs from the simple penetration type (a). The following is a summary of the applicable range:

GMAW of the simple penetration type.
Operating parameter n ≤15.
Weaving of 2 mm and less.
Plate thickness of 5 mm and above.

Summary

This study uses the classical heat conduction solution with an assumption of a moving point heat source for the analysis of the fusion area, depth, and width in GMAW. The results of comparison with experimental fusion depth and width show systematic errors. These were corrected by corrections based on regression equations. The resulting semiempirical weld model shows good agreement with experimental data for both bead-on-plate welds and T-joint fillet welds. Moreover, the methodology using this semiempirical approach can be extended to practical prediction of weld fusion for materials other than steel.

The following conclusions have been obtained from this study:

While giving prediction errors in fusion depth and width, the theoretical heat conduction solution using a moving point heat source provides good qualitative agreement for the fusion area. This introduces the arc efficiency through fusion area for each welding position through theoretical and bead-on-plate weld comparisons.

The corrected solution also provides a good approximation of fusion depth and width by reducing the systematic errors between theory and experiments. The regression equations show good correlation with experimental data for bead-on-plate welds. This results in development of a reliable model for prediction of fusion.

This study also analyzes fusion depth and width in T-joint fillet welds using the same model. The model can predict fusion depth and width well for both web and flange by adopting an assumed heat distribution ratio and effect of reflected heat on the end surface of web.

The model provides prediction for fusion depth and width in GMAW in an easy and practical manner. It will be useful in the design of welding procedures and in adaptive control of welding parameters in automated welding systems.

This semiempirical weld model can be ex-

tended using the developed methodology to a wider range of operating parameters with ancillary experimentation.

Acknowledgments

This research was funded by the Office of Naval Research (ONR). The authors are grateful to John Carney, Office of Naval Research (ONR), who supported and encouraged the research. The opinions are those of the authors and do not represent the views of the ONR. The authors are grateful to Koichi Masubuchi, professor emeritus of Massachusetts Institute of Technology, who gave us valuable advice. The authors also appreciate the efforts of Brian Baughman of the Edison Welding Institute who performed the experiments and Robert Latorre, professor, University of New Orleans, for his comments on the manuscript.

References

1. Christensen, N., Davies, V. de L., and Gjermundsen, K. 1965. Distribution of temperature in arc welding. *British Welding Journal* (2): 54s–75s.

2. Ando, K. 1967. Calculation of temperature in molten pool of welding arc. *Welding Journal of Japan Welding Society* 36(3): 252s–260s.

3. Eagar, T. W., and Tsai, N. S. 1983. Temperature fields produced by traveling distributed heat sources. *Welding Journal* 62(10): 346-s to 355-s

4. Ohwa, T. 1956. Shape of penetration (report 1) — Homogeneous thermal distribution in arc welding. *Welding Journal of Japan Welding Society* 25(9): 492s–497s.

5. Ohwa, T. 1957. Shape of penetration (report 2) — Shapes observed. *Welding Journal of Japan Welding Society*, Vol. 26.

6. Woods, R. A., and Milner, D. R. 1971. Motion in the weld pool in arc welding. *Welding Journal* 50(4): 163-s to 173-s.

7. Ishizaki, K., Okada, T., and Yokoya, S. 1994. Electromagnetic force near anode boundary and double convection in TIG arc weld pool. *Quarterly Journal of Japan Welding Society* Vol. 12, pp. 200s–206s.

8. Hiraoka, K., Okada, A., and Inagaki, M. 1985. Effect of helium gas on arc characteristic in gas tungsten arc welding. *Quarterly Journal of Japan Welding Society*, 3(2): 241s–246s.

9. Hiraoka, K., Okada, A., and Inagaki, M. 1985. Effect of helium gas on arc characteristic in gas tungsten arc welding. *Quarterly Journal of Japan Welding Society*, 3(2): 246s–252s.

10. Friedman, E. 1978. Analysis of weld puddle distortion and its effect on penetration. *Welding Journal* 57(6): 161-s to 166-s.

11. Heiple, C. R., and Roper, J. R. 1982. Mechanism for minor element effect on GTA fusion zone geometry. *Welding Journal* 61(4): 98-s to 102-s.

12. Heiple, C. R., Roper, J. R., Stagner, R. T., and Aden, R. 1983. Surface active element effects on the shape of GTA, laser, and electron beam welds. *Welding Journal* 62(3): 72-s to 77-s.

13. Hirata, Y., Asai, Y., Takenaka, K., Kunishige, S., Ohgaki, S., Miyasaka, F., and Ohji, T. 2002. 3D – Numerical Model Predicting Penetration Shape in GTA Welding, IIW Doc., 212-1023-02.

14. Kou, S., and Wang, Y. H. 1986. Weld pool convection and its effects. *Welding Journal* 65(3): 63-s to 70-s.

15. Tsao, K. C., and Wu, C. S. 1988. Fluid flow and heat transfer in GMA weld pool. *Welding Journal* 67(3): 70-s to 75-s.

16. Yokoya, S., Okada, T., and Matsunawa, A. 1994. Welding of carbon steels in stationary TIG arc. *Quarterly Journal of Japan Welding Society* 12(2): 192s –199s.

17. Zacharia, T., Eraslan, A. H., and Aidun, D. K. 1988. Modeling of nonautogeneous welding. *Welding Journal* 67(12): 510-s to 519-s.

18. Zacharia, T., David, S. A., Vitec, J. M., and DebRoy, T. 1989. Weld pool development during GTA and laser beam welding of Type 304 stainless steel, part 2 — Experimental correlation. *Welding Journal* 68(12): 510-s to 519-s.

19. Essers, W. G., and Walter, R. 1981. Heat transfer and penetration mechanisms with GMA and plasma–GMA welding *Welding Journal* 60(2): 37-s to 42-s.

20. Ando, K., Nishikawa, J., and Wada, H. 1968. A consideration on the mechanism of penetration in arc welding. *Welding Journal of Japan Welding Society* 37(4): 359-s to 368-s.

21. Mendez, P. F., and Eagar, T. W. 2003. Penetration and defect formation in high-current arc welding. *Welding Journal* 82(10): 296-s to 306-s.

22. Ando, K., Nishikawa, J., and Wada, H. 1968. A consideration on the mechanism of penetration in arc welding. *Welding Journal of Japan Welding Society* 37(4): 359-s to 368-s.

23. Cao, Z., Yan, Z., and Chen, X. C. 2004. Three-dimensional simulation of transient GMA weld pool with free surface. *Welding Journal* 83(6): 169-s to 176-s.

Preparation of Manuscripts for Submission to the *Welding Journal* Research Supplement

All authors should address themselves to the following questions when writing papers for submission to the Welding Research Supplement:

- ◆ Why was the work done?
- ◆ What was done?
- ◆ What was found?
- ◆ What is the significance of your results?
- ◆ What are your most important conclusions?

With those questions in mind, most authors can logically organize their material along the following lines, using suitable headings and subheadings to divide the paper.

1) **Abstract.** A concise summary of the major elements of the presentation, not exceeding 200 words, to help the reader decide if the information is for him or her.

2) **Introduction.** A short statement giving relevant background, purpose, and scope to help orient the reader. Do not duplicate the abstract.

3) **Experimental Procedure, Materials, Equipment.**

4) **Results, Discussion.** The facts or data obtained and their evaluation.

5) **Conclusion.** An evaluation and interpretation of your results. Most often, this is what the readers remember.

6) **Acknowledgment, References and Appendix.**

Keep in mind that proper use of terms, abbreviations, and symbols are important considerations in processing a manuscript for publication. For welding terminology, the *Welding Journal* adheres to AWS A3.0:2001, *Standard Welding Terms and Definitions.*

Papers submitted for consideration in the Welding Research Supplement are required to undergo Peer Review before acceptance for publication. Submit an original and one copy (double-spaced, with 1-in. margins on 8 1/2 x 11-in. or A4 paper) of the manuscript. A manuscript submission form should accompany the manuscript.

Tables and figures should be separate from the manuscript copy and only high-quality figures will be published. Figures should be original line art or glossy photos. Special instructions are required if figures are submitted by electronic means. To receive complete instructions and the manuscript submission form, please contact the Peer Review Coordinator, Erin Adams, at (305) 443-9353, ext. 275; FAX 305-443-7404; or write to the American Welding Society, 550 NW LeJeune Rd., Miami, FL 33126.